Eilif Müller

Simulation of High-Conductance States
in Cortical Neural Networks

Masters thesis

HD-KIP-03-22

KIRCHHOFF-INSTITUT FÜR PHYSIK

Simulation of High-Conductance States
in Cortical Neural Networks

This Masters thesis was carried out by Eilif Müller

at the Kirchhoff-Institut für Physik

under the supervision of

Herr Prof. Dr. Karlheinz Meier

Abstract

Simulation of High-Conductance States in Cortical Neural Networks

A network simulation paradigm was developed to be consistent with cortical neurons in the high-conductance state of an awake brain *in-vivo*. Two classes of integrate-and-fire based neurons, pyramidal (with adaptation) and inhibitory, were modeled. Synapses were conductance based. The high-conductance state is induced by synaptic bombardment with 1000 excitatory and 250 inhibitory Poisson processes. Following the network init phase, the network synapses are enabled, replacing a fraction of the Poisson process input. The idea of model-consistent background rates was introduced to resolve the issue that each neuron is part of its own background in recurrent networks with persistent activity. A 9x9x9 grid of neurons with a cortex inspired network topology was simulated at 1/200th real-time. Coherent network bursting was observed at $\sim$ 5-7 Hz. The dependence of the burst period on the decay constant of adaptation was demonstrated to be linear with a slope consistent with unity. The simulation is event based and scalable to a Linux cluster implementation.

Simulation von Zustaenden stark erhoehter Leitfaehigkeit in cortikalen neuronalen Netzen

Es wurde ein Paradigma fuer eine Netzwerksimulation entwickelt, welches mit dem Zustand stark erhoehter Leitfaehigkeit cortikaler Neuronen konsistent ist, wie er in-vivo im wachen Gehirn vorliegt. Zwei Klassen von auf dem ïntegrate-and-fireModell basierenden Neuronen wurden modelliert: pyramidale (mit Adaptation) und inhibitorische. Alle Synapsen sind leitwertbasiert. Der Zustand stark erhoehter Leitfaehigkeit wird durch ein synaptisches Bombardement mit 1000 erregenden und 250 hemmenden Poissonprozessen erzeugt. Nach einer Einschwingphase werden die Synapsen des Netzwerkes aktiviert und ersetzen einen Teil der Poissonprozesse. Der Ansatz einer modellkonsistenten Hintergrundaktivitaet wurde entwickelt, um das Problem staendig aktiver, rueckgekoppelter Netzwerke zu loesen, naemlich dass jedes Neuron einen Teil zu seiner eigenen Hintergrundaktivitaet beitraegt. Simuliert wurde ein Gitter aus 9x9x9 Neuronen mit einer an den Cortex angelehnten Topologie. Es wurden kohaerente Pulsgruppen mit einer Frequenz von 5 bis 7 Hz beobachtet. Es konnte gezeigt werden, dass die Abhaengigkeit der Periode dieser Gruppen von der Adaptationszeitkonstante linear mit einer Steigung von eins ist. Die Simulation ist ereignisbasiert programmiert und kann auf einen Linux Parallelrechner uebertragen werden.

„Der Mensch, die wohl geheimnisvollste Spezies unseres Planeten. Ein Mysterium offener Fragen. Wer sind wir? Woher kommen wir? Wohin gehen wir? Woher wissen wir, was wir zu wissen glauben? Wieso glauben wir überhaupt etwas? Unzählige Fragen, die nach einer Antwort suchen, einer Antwort, die wieder eine neue Frage aufwerfen wird, und die nächste Antwort wieder die nächste Frage und so weiter und so weiter. Doch ist es am Ende nicht immer wieder die gleiche Frage, und immer wieder die gleiche Antwort? "

–"Lola rennt", Tom Tykwer

Contents

Introduction

The neuron is generally considered the basic element of the complex dynamical system we call the brain, the vast network of interconnected neurons which manifests will and intellect.

Much effort has been exerted in recent times to understand the neuron, and the efforts have been aptly rewarded. The are many excellent books which describe neuronal modeling in exquisite detail [1–3].

But our understanding falls short when it comes to large networks of neurons. Analytical breakthroughs are seldom as the problem is virtually intractable except in cases too simple to be relevant. Simulation provides a viable alternative. With the aid of modern computer simulations such as NEURON [4], many aspects of observed neuronal behavior can be accurately reproduced. However, the treatment of large biologically realistic networks of neurons using simulation is notably infrequent. Their functionality is largely a mystery and metrics to evaluate performance are absent while classical learning architectures such as attractor networks are inappropriate, extraneous and archaic [5].

Recent advancements in our understanding of cortical neuron behavior *in-vivo*, notably, the characterization of the so called *high-conductance* state, could provide a piece of the puzzle that will bring network simulations more relevance. The high-conductance state, an activated state due to ongoing synaptic bombardment from neighboring neurons, has been observed in both experiment and simulation [6, 7], and provides a target mode of operation for realistic network simulations.

In the pages to follow, a paradigm for simulating small populations of inter-connected neurons operating in high-conductance states will be described. The goal is to provide further insight into the key questions of cortical neural networks: persistent activity and stability [1, pp. 417]; the significance of the high-conductance state and background network activity [7–9]; and emergent properties of networks as influenced by the chosen neuron model, network topology, synaptic plasticity and neuromodulation mechanisms [10–12].

The project is intended to parallel the development of a hardware integrate-and-fire-like neural network implementation also currently under development in the group, and supply that development process with parameters and design constraints. Additionally, the software infrastructure used to test the simulation and perform the experiments described here will form the test bed for the hardware upon completion.

Chapter 1

Single Neuron Models

The integrate-and-fire (I&F) model was chosen for its efficiency as the goal is to simulate large networks of neurons. Two classes of neurons, pyramidal (PY,excitatory) and inhibitory (IN) where chosen as distinct. Synapses were modeled as conductance based with simple discontinuous onset and exponential decaying conductances for the two neurotransmitter types included, AMPA[1] (excitatory) and $GABA_A$[2](inhibitory) [7, 8].

In this chapter, using the NEURON simulation environment [4], building on scripts and model code provided by A. Destexhe [13], Hodgkin-Huxley (HH) based compartment models [3], were compared to the I&F models. Additional mechanisms accounting for spike-rate-adaptation (only pyramidal neurons) and relative refractory periods were added to the I&F models which were subsequently fit to the HH models under various single and double neuron simulations. Let us now go into detail.

1.1 The Basic I&F Model

The ubiquitous Integrate-and-Fire (I&F) model of the neuron can be found in any quality spiking neuron textbook with little variation [1–3]. For completeness and a definition of terms, the I&F model is described here, with further details and the exact parameters used left to appendix A.

As is generally the case for all spiking neuron models, the I&F model takes the form of a first order differential equation where the rate of change of the membrane potential of the cell body, v, is related to various membrane currents. Specifically for the I&F model used,

$$c_m \frac{dv(t)}{dt} = g_l(E_l - v(t)) + \sum_j \frac{w^j g_s^j(t)}{A}(E_s^j - v(t)),$$ (1.1)

Where the sum over j is the sum over all synapses.

If v exceeds the *threshold voltage*, v_{th}, v is reset to v_{reset} for a time τ_{ref} and an action potential (AP) event is generated. The AP event triggers synaptic release events at the neuron's synapses following a small delay to model propagation time.

Parameters:

- v_{th} - threshold voltage

- v_{reset} - reset voltage

- τ_{ref} - absolute refractory period

- c_m - specific membrane capacitance

---

[1]AMPA is short for α-amino-3-hydroxy-5-methyl-4-isoxalone propionic acid [3].
[2]GABA is short for γ-aminobutyric acid [3].

- g_l - specific membrane leak conductance

- E_l - membrane reversal potential

- $g_s^j(t)$ - conductance due to synapse j

- E_s^j - reversal potential of synapse j

- w^j - synaptic weight

- A - membrane surface area

For a given synapse j, an AP event at the presynaptic neuron at time t_{ap} triggers a synaptic release event at time $t_{ap} + t_{delay}^j$, a discontinuous increase in the synaptic conductance,

$$g_s^j(t_{ap} + t_{delay}^j + dt) = g_s^j(t_{ap} + t_{delay}^j) + q_s^j,$$

otherwise $g_s^j(t)$ is governed by,

$$\frac{dg_s^j(t)}{dt} = \frac{-1}{\tau_s^j} g_s^j(t).$$

Parameters:

- q_s^j - quantal conductance increase

- τ_s^j - synaptic decay time

- t_{delay}^j - presynaptic-neuron-to-synapse AP propagation delay

For all experiments to follow, the synaptic weights, w^j, were set to unity. This parameter has been included with weight variation experiments such as long term synaptic plasticity in mind. Equivalently, one could instead vary q_s and drop one parameter from the model. This may change in the near future in favor of the form found to be most convenient to implement biologically plausible synaptic plasticity experiments.

1.2 Fitting the I&F to the HH Model in NEURON

The simple I&F model presented in eq. 1.1 consists of $1 + n_s$ coupled differential equations and $7 + 4n_s$ independent parameters per neuron with n_s synapses (see Appendix A for a summary). The methods used to adjust the I&F model and its parameters to maximize its consistency with the biological reality will now be presented.

The HH and I&F models have similarities. They have identical passive membrane properties (leak mechanisms, etc.) and synaptic models, both have voltage dependant firing mechanism, and both have a period of dormancy following spike events. To say, however, that the I&F model captures all important aspects of HH behavior would be generous. During a handful of single and paired neuron experiments, I&F parameters were varied to achieve optimum agreement to the HH model. Although behavior was often qualitatively similar, quantitative agreement was in most cases only achieved by sacrificing agreement in another situation. In what follows, the various experiments will be presented in chronological order so that the reader can follow the changes to the I&F model and parameters as it converges to the final form.
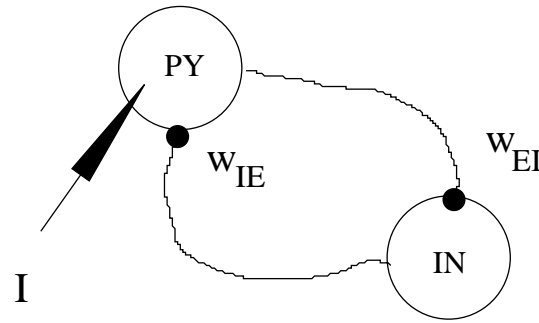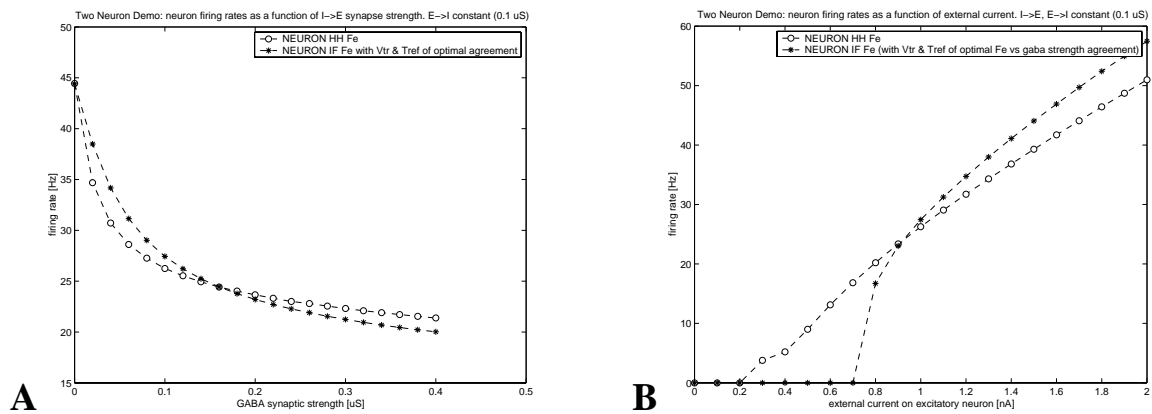
Figure 1.1: A schematic of the two-neuron model.

Figure 1.2: **A**: two neuron experiment f-vs-w_{IE}, HH model and I&F best fit with respect to v_{th} and τ_{ref}. **B**: two neuron experiment f-vs-I, HH model and I&F with parameters as in A.

1.2.1 Comparison 1: The two-neuron experiment

The first comparison between the HH and I&F models was the two-neuron experiment of A. Destexhe. In this experiment a single pyramidal neuron is presynaptic to an excitatory synapse of peak conductance w_{EI} located on an inhibitory neuron which in turn is presynaptic to an inhibitory synapse of peak conductance w_{IE} located on the pyramidal neuron. The pyramidal neuron is then injected with a constant current I. A schematic is shown in fig. 1.1.

With the excitatory peak conductance, w_{EI}, and the injected current, I, set to constant values 0.1μS and 1.0nA respectively, the inhibitory conductance , w_{IE}, was varied and the firing rate of the PY neuron was measured. Fig. 1.2A shows both HH and I&F models, where v_{th} and τ_{ref} of the I&F model were varied to attain an optimal fit. The membrane parameters of the I&F model were set equal to the HH model and $v_{reset} = -75$mv. A fit of the HH+I_M model proved impossible. The low steady states firing rates of the HH+I_M could not be achieved without unreasonable I&F leak conductances.

Fig. 1.2B shows the firing rate as a function of I for both HH and I&F, where the I&F parameters were left unchanged from the previous fit. Clearly the reasonable fit for $I = 1.0$nA in fig. 1.2A is a poor fit for $I = 0.5$nA. This lack of fit generality was characteristic throughout the fitting procedure. Even more discouraging was the total failure of a reasonable fit for the HH model including the I_M current. We shall see in the chapters to follow that this mechanism, which is responsible for spike rate adaptation, is an important aspect of pyramidal neurons. It does not make sense to neglect it here.
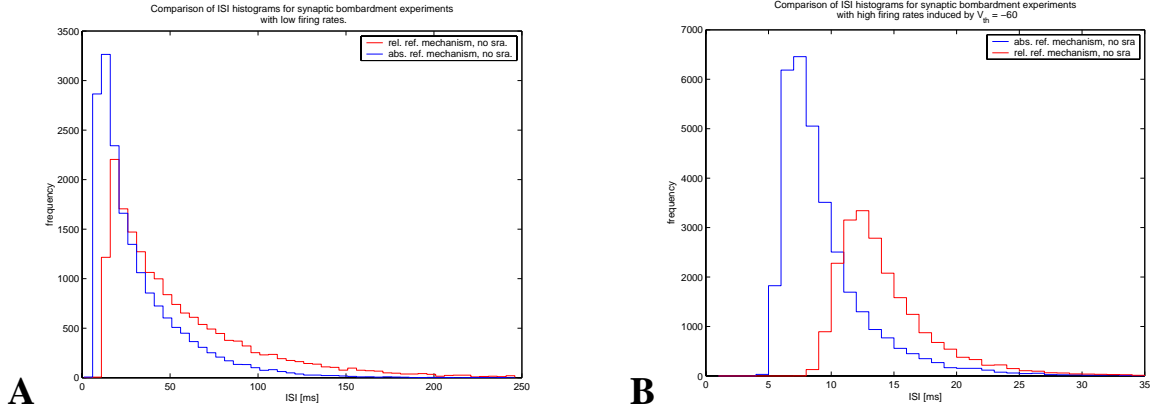
Figure 1.3: I&F ISI histograms comparing absolute to relative refractory mechanisms **A**: Low firing rate. **B**: High firing rate.

1.2.2 Comparison 2: ISI histograms under synaptic bombardment

Inter-spike interval (ISI) histograms of non-bursting cortical pyramidal cells *in-vivo* show characteristically gamma-like distributions, with a sharp but smoothly decreasing probability for shorter intervals and an exponentially decaying probability for larger intervals [1, ch. 15]. HH+I_M based models for pyramidal neurons under synaptic bombardment experiments can be shown to reproduce gamma-like ISI histograms [8]. By bombarding the I&F model with 1000 excitatory and 250 inhibitory Poisson process activated synapses of peak conductance $q_s = 0.002 \mu S$ *in-vivo* activity can be simulated [6,7]. The ISI histogram for the I&F model under these simulated *in-vivo* conditions is that for the absolute refractory mechanism shown in fig. 1.3A. It has an exponential ISI distribution like that of the Poisson process driving the synapses.

A relative refractory (relref) period mechanism was added to the I&F model of the form suggested in [1, pp. 339] with hopes it would improve agreement with the HH+I_M gamma-like ISI behavior. The mechanism consists of a current, $g_{relref}(t)$, which decays exponentially to zero with time constant $\tau_{relref} \approx \tau_{ref}$,

$$\frac{dg_{relref}(t)}{dt} = \frac{-1}{\tau_{relref}} g_{relref}(t),$$

and is discontinuously increased,

$$g_{relref}(t_{ap} + dt) = g_{relref}(t_{ap}) + q_{relref},$$

following an AP event of the cell at t_{ap}. It was included in the membrane potential differential equation as an additional conductance term with reversal potential E_{relref}. Eq. 1.1 then becomes:

$$c_m \frac{dv(t)}{dt} = \cdots + g_{relref}(t)(E_{relref} - v(t)). \tag{1.2}$$

Parameters:

- q_{relref} - relref quantal conductance increase

- τ_{relref} - relref conductance decay time

- E_{relref} - relref reversal potential

To investigate the effects of the relref mechanism on the ISI histogram, further synaptic bombardment experiments were performed for the I&F+relref model. For low firing rates, as those in fig. 1.3A, the ISI histograms with and without the relref mechanism were found to be marginally different. A deviation was found only for higher firing rates, as shown in fig. 1.3B.

Although a slight improvement is hinted at with the addition of the relref mechanism, it is hardly convincing. However, as we will see later, networks of neurons were shown to exhibit short coherent explosions of activity. In these situations, were the neurons are being strongly excited by the network, a relref mechanism does not exclude shorter than normal refractory periods and thus could magnify the explosion, in contrast to the absolute mechanism which has a static refractory period independent of excitation from the network. This aspect of the relative refractory period mechanism resulted in it being favored over absolute refractory mechanisms in the implementation of the simulation. Although the comparisons are admittedly somewhat inconclusive, it will not be investigated further here. Further work could include a more thorough study of the role of the relative refractory period on the coherent network bursting observed.

1.2.3 Comparison 3: single neuron f-vs-I curves

The key distinction between the HH based models of the pyramidal neuron and the inhibitory neuron provided by A. Destexhe was the inclusion of an $I_M{}^3$ current mechanism in the pyramidal neuron model. By this mechanism, each AP event in the pyramidal neuron opens specific ion channels causing a depolarizing current which persists for ≈ 100ms. The effect of the mechanism on periodic spiking of the cell is a decrease in the spiking frequency with time, know as *spike rate adaptation* or simply *adaptation* [3, 14].

The absence of an I_M current-like adaptation mechanism in the I&F model in eq. 1.1 was already quite clear in the two-neuron experiments of our first comparison.

To remedy the impossible agreement between I&F and HH+I_M seen there, a spike-rate-adaptation (sra) mechanism was added to the I&F model of the same form as the relref mechanism mentioned in the previous section but with a smaller quantal conductance increase and a much larger decay time. Eq. 1.2 then becomes:

$$c_m \frac{dv(t)}{dt} = \cdots + g_{sra}(t)(E_{sra} - v(t)),$$ (1.3)

with $g_{sra}(t_{ap} + dt) = g_{sra}(t_{ap}) + q_{sra}$ and $\frac{dg_{sra}(t)}{dt} = \frac{-1}{\tau_{sra}} g_{sra}(t)$ as for the relref mechanism. Parameters:

- q_{sra} - sra quantal conductance increase

- τ_{sra} - sra conductance decay time

- E_{sra} - sra reversal potential

The two-neuron comparison was abandoned temporarily in favor of simpler single neuron firing rate vs I experiments. As the steady state firing rate of models with adapting mechanisms is slower than the initial firing rates, reciprocal ISI intervals of specific ISI pairs (first, second, third, etc.) were used to give an estimate of the instantaneous firing frequency during adaptation. By comparing the f-vs-I curves for HH+I_M and I&F+sra+relref, optimal values for the sra and relref parameters were found using the `praxis` optimization method of a `MultiRunFitter` under NEURON. Shown in fig. 1.4 are the HH and I&F curves for the first, second and third ISI pairs using these optimal values. Also shown is the dismal agreement when the sra mechanism is absent. Clearly the sra mechanism is doing much to improve the agreement of the I&F model to HH+I_M.

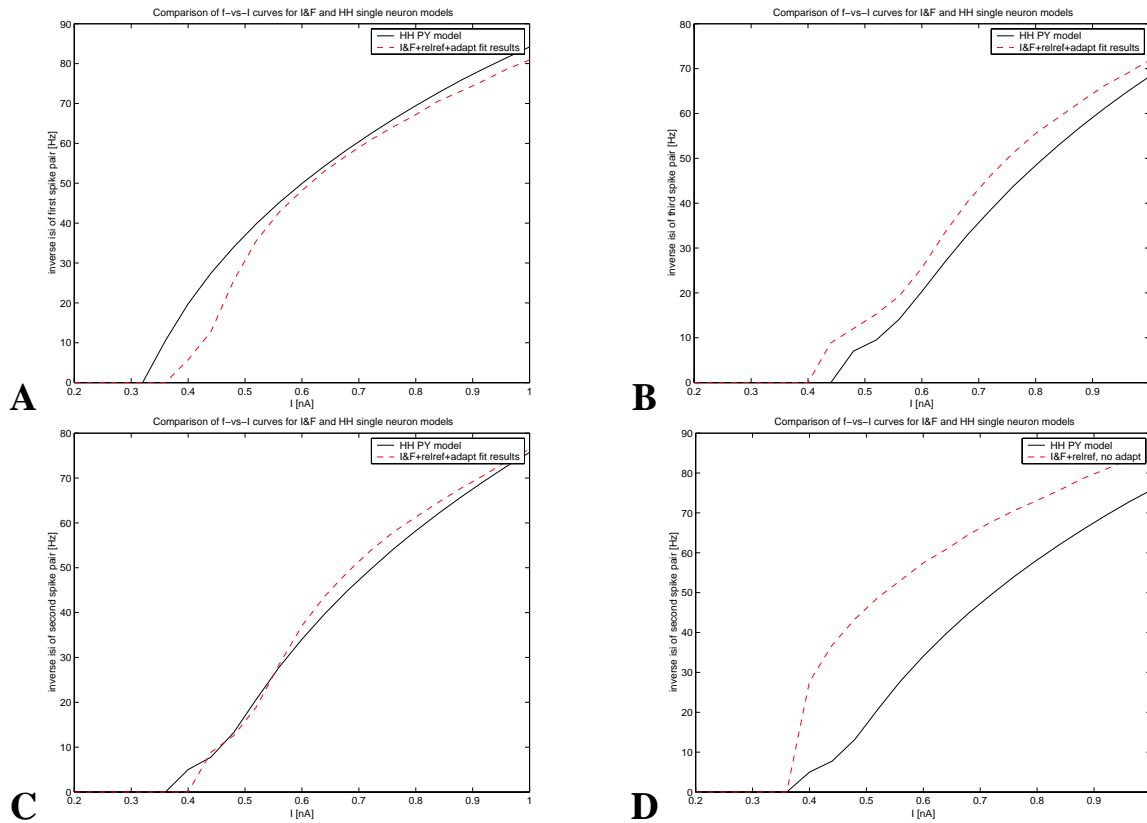[3]The M stands for muscarine, the application of which leads to the inhibition of this current [14].

Figure 1.4: **A**: two neuron experiment f-vs-I, HH+I_M model and I&F+sra+relref. The ISI of the first spike pair was used to estimate the frequency. **B**: frequency estimated using the ISI of the third spike pair, otherwise same as in A. **C**: The ISI of the second spike pair was used, otherwise same as in A. **D**: The ISI of the second spike pair was used and sra was turned of in the I&F model, otherwise same as in A.
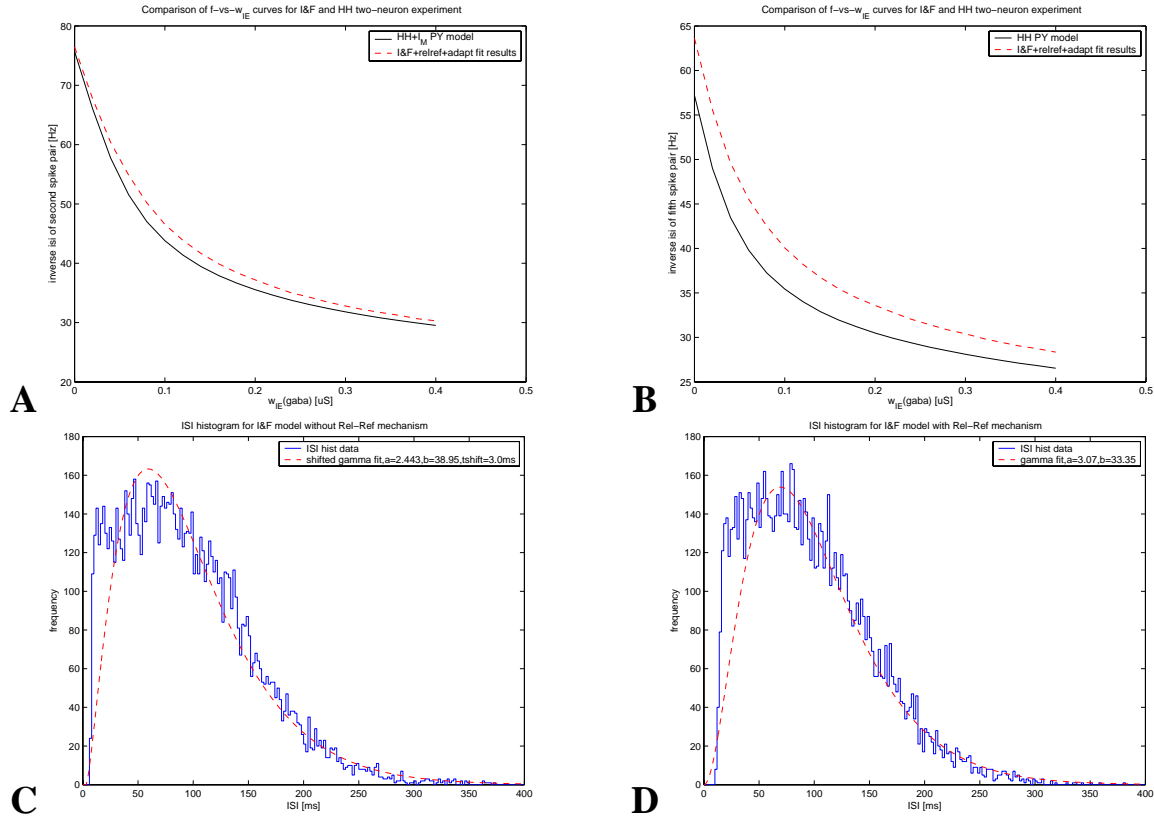
Figure 1.5: **A**: two neuron experiment f-vs-w_{IE}, HH model and I&F+relref+sra model using best fit parameters as for the f-vs-I curves in fig. 1.4. f is measured wrt. the second spike pair. **B**: same experiment as in A, but with f measured wrt. the fifth spike pair. **C**: I&F+sra ISI histogram. **D**: I&F+sra+relref ISI histogram.

Using the I&F+sra+relref parameters determined by the fit in fig. 1.4 (see appendix A for the exact values used), comparisons of the previous sections were revisited to test the generality of the fit.

For the two-neuron model, as before, the network architecture is as in fig. 1.1. The instantaneous frequency is, as for the f-vs-I experiments, measured by reciprocal ISI intervals of specific spike pairs. For the second and fifth spike pairs, the results are shown in figs. 1.5A,B. Where agreement without sra was impossible, it is now reasonably good without fitting beyond that done with the f-vs-I curves.

For the same model and parameters, the ISI histogram under *in-vivo*-like synaptic bombardment is shown in figs. 1.5C,D (once without relref mechanism, once with). The appreciable change in the ISI distribution is clear. The shift towards the gamma-like variability of experimental observations and the HH+I_M model under similar experiments is favorable.

Indeed, improvements in agreement between the HH+I_M and the I&F model are demonstrated on multiple fronts, indicating a measure of generality of the fit parameters and reinforcing the sra mechanism as a step in the right direction.

1.2.4 Comparison 4: synaptic bombardment firing comparison

The firing rate of the I&F model under synaptic bombardment is strongly dependant on the threshold voltage, v_{th}, as seen in fig. 1.6. By bombarding the synapses of the HH+I_M and I&F+sra+relref mod-

els with the same event train (they were run simultaneously), v_{th} was adjusted by hand to match firing rates of the two models. Surprisingly, it was found that the two models fire almost simultaneously with $v_{th} \approx -57$mV for the pyramidal neuron and $v_{th} \approx -54.5$mV for the inhibitory neuron. Other parameters determined through the previous comparisons were used. For the pyramidal neuron, this fact is shown in fig. 1.7.

A notable difference which has yet gone unmentioned is the difference of AP generation mechanisms of the two models. While for I&F one has a "hard" threshold mechanism, the bifurcation responsible for AP events in the HH model is likely "softer". In synaptic bombardment experiments, the membrane potential undergoes a random walk around its mean. In the case of I&F, spiking occurs if the membrane potential crosses the threshold voltage, end of story. In the case of HH, if the membrane potential "jumps" across a threshold and quickly jumps back, a spike might not occur where it would if it "walked" across. Speculatively speaking, this softening of the thresholding mechanism might account for some instances in which the I&F mechanism fires where HH did not. Other instances are likely due to the remaining discrepancies in the adaptation and refractory mechanisms of the two models.

1.3   Conclusions and Outlook

After a barrage of tests, the I&F model looks considerably different. Significant is the addition of an adaptation mechanism and a relative refractory period mechanism. Biologically plausible parameter sets for the pyramidal and inhibitory neuron classes have been attained through automatic and manual fitting to the HH model and are summarized in appendix A. They are consistent with the "literature means". Agreement with the HH benchmark is satisfactory at best, and sometimes quite poor. However, the HH simulations of neurons may or may not represent the "form" of a neuron in a Platonic sense. Certainly in the future it will be clear, some unimportant details are eluding other important ones. What aspects of the neuron are pertinent is a question necessarily answered by understanding how the neuron behaves in a network. Progress will likely come as an iterative process of neuron model to network to new neuron model. For this reason, we will leave the problem of neuron modeling to rest and shift the investigation towards simulation of large networks of neurons of the current model.

As we move to examining networks dynamics it may be useful to keep some unanswered modeling questions in mind. How might the I&F model be improved by softer spiking mechanisms? Additional adaptations mechanisms could be investigated to better fit f-vs-I behavior. More elaborate fitting schemes which adjust the relref and sra parameters to improve simultaneous spiking during synaptic bombardment experiments could be explored.
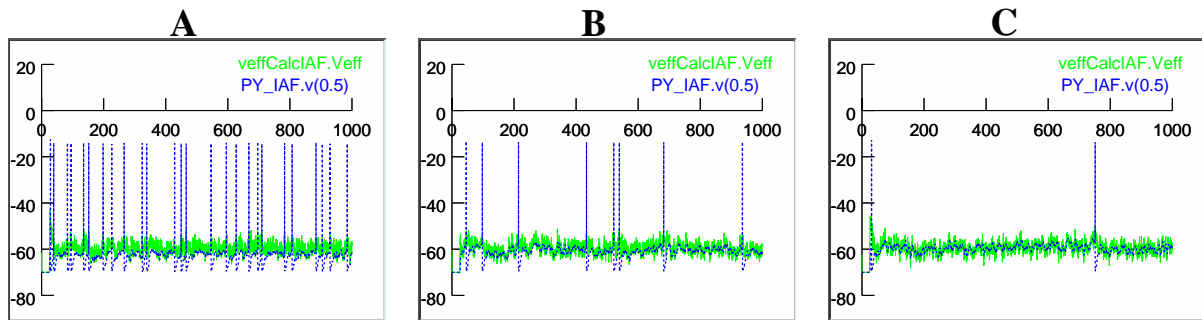
Figure 1.6: I&F+sra+relref model with 1000 excitatory,(250 inhibitory) Poisson process synapses with rate of 8.9Hz,(15.5Hz) and quantal conductance increase of $0.002\mu S$,($0.002\mu S$) simulated in NEURON. **A**: $v_{th} = -60$mv. **B**: $v_{th} = -57$mv. **C**: $v_{th} = -55$mv.
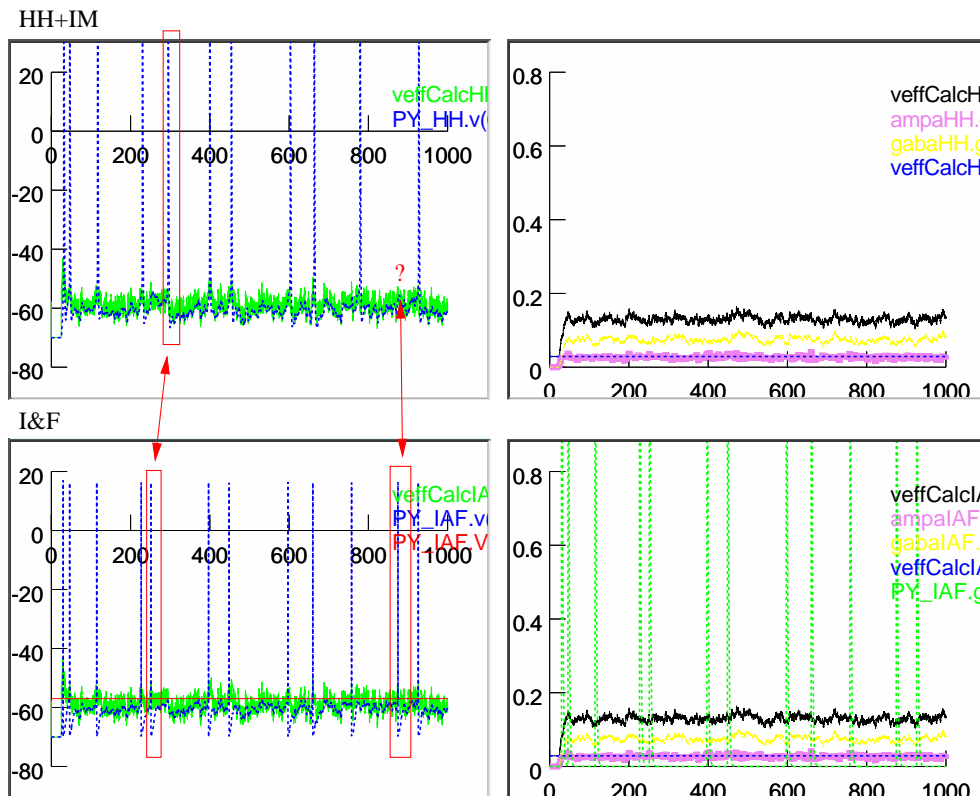

Figure 1.7: The near simultaneous behavior of the I&F+sra+relref and HH+I_M models for $v_{th} = -57$mv. Other I&F parameters as determined by previous comparisons.

Chapter 2

Simulating Neurons in HANNEE

The implementation of a simulation of the neuron models discussed in the previous chapter was undertaken in native C++ expanding on the HANNEE framework currently under development at the Electronic Vision(s) group of the Kirchhoff-Institut für Physik, Ruprecht-Karls-Universität Heidelberg. It was designed with simulation of large networks of neurons in mind, which will be discussed in chapters to follow. The choice of HANNEE as a base for the simulation will allow interchangeability of simulated networks with future hardware network implementations with regard to the various experiments developed to investigate neuron and network behavior. Additionally the undertaking has benefited from and contributed to the accumulation of knowledge HANNEE represents.

2.1   Introduction to HANNEE

The Hardware Analog Neural Network Evolution Environment, or HANNEE is an object oriented interactive application custom built to control various neural network experiments and learning algorithms for the mixed-signal neural network integrated circuits under development in the Electronic Vision(s) group. The object manager, shown in fig. 2.1 is the main window of HANNEE.

HANNEE implements a hardware abstraction layer (HAL), by which experiments written in the framework can interact with a generalization of a simulation engine without dealing with the messy details of communicating with hardware. The HAL takes the form of the `HNetMan` object, shown in fig. 2.2, which provides the `HNetData` object to all experiments which require it. HNetMan allows choice of hardware and configuration of all hardware specific settings. HNetData is an abstract class by which all variables which are interesting for an experiment can be set using an intuitive interface hidden from hardware internals. HNetData is inherited by hardware network chip specific classes, one for each distinct type. The internals of these classes provide the link between software and hardware.

2.2   Expanding on HANNEE

To add spiking neuron simulation capabilities to the HANNEE framework, an additional chip class named `HSpikeChipData` was added to the HNetData inheritance hierarchy. This object is an abstract class from which all spiking neural network implementations, hardware or simulation, should be derived.

The `HSimSpikeConData` class implements the specifics of the conductance-based integrate-and-fire model simulation as described in chapter 1. As helper classes it employs `NeuronCon` and `Synapse`, which store the states of neurons and synapses, and implement the numerical integration of dynamical equations.

To date, three experiments have been written which use the `HSimSpikeConData` simulation to investigate the behavior of neurons and networks. The `TwoNeuronAlgo` object is an experi-
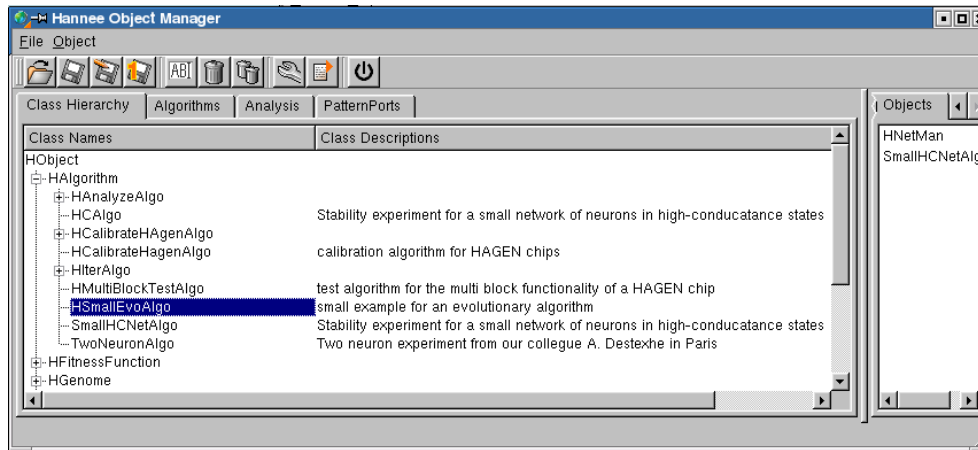
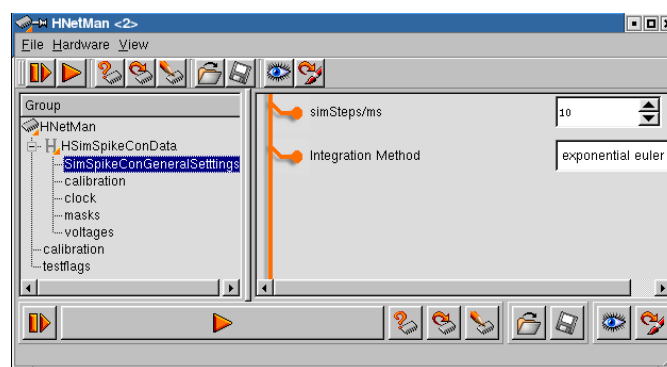Figure 2.1: The object manager, the main window of HANNEE

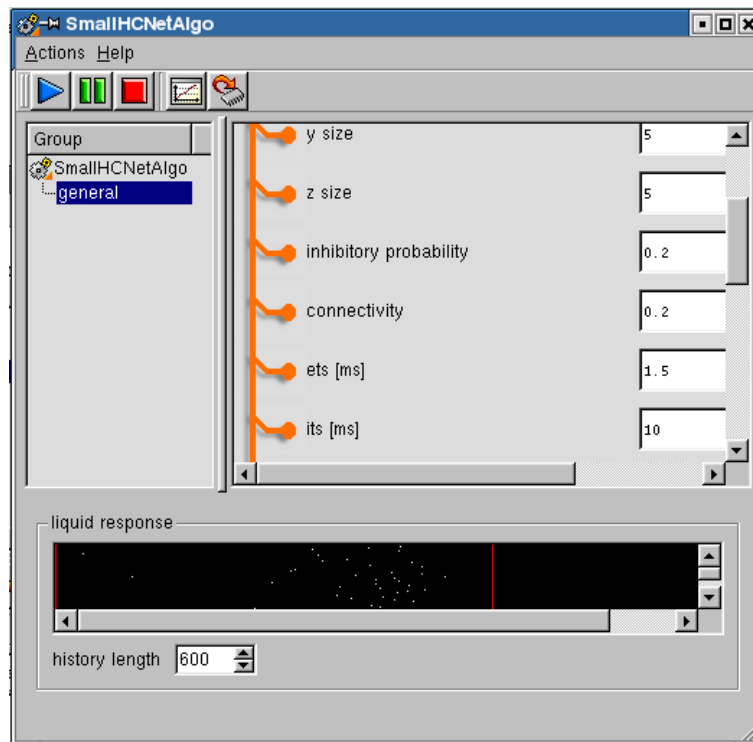Figure 2.2: The interactive window of the HNetMan object.

Figure 2.3: The interactive window of the SmallHCNetAlgo object.

ment which implements the two-neuron experiment described in section 1.2.1. The `HCAlgo` object implements a synaptic bombardment experiment for a single neuron used to investigate the high-conductance state. The `SmallHCNetAlgo` implements a small network of interconnected neurons in high-conductance states, the details and results of which make up chapter 3. The `SmallHCNetAlgo` object window is shown in fig. 2.3

2.3 Synapse Event Queues

The `HSimSpikeConData` simulation implements an event based signaling scheme. When an action potential event occurs for a specific neuron, synaptic release events are triggered in the neuron's synapses by placing a release time equal to the current time plus the transmission delay in the *event queue* of each of the synapses. This has the advantage that neuron spiking histories are not required to implement network delays, and that each neuron with synaptic inputs is autonomous except during signaling events, improving efficiency. Simulation of Poisson process synaptic background works in a similar fashion. Although spike-time-dependent plasticity rules are yet unimplemented, an extension of the queue scheme is forseen which is compatible with this paradigm. It is forseen to exploit the autonomy of the simulation objects to allow efficient simulation of large cortical networks on Linux clusters with relatively minimal network bandwidth requirements.

2.4 Numerical Methods

As the membrane equation is a differential equation in time, solving it in simulation requires a numerical integration scheme of some sort. The `HSimSpikeConData` based simulation implements the *forward Euler* and the *exponential Euler* integration schemes, from which the user can choose.

The *forward Euler* integration scheme is the simplest method for numerical integration. Given

$$\frac{dy}{dt} = f(x, t),$$

the solution at a time $t + dt$ where dt is the *time step of integration*, is approximated in terms of the solution at time t by:

$$y(t + dt) = y(t) + f(x, t)dt.$$

Although this method is simple and efficient, it is quite unstable and requires a small time step of integration for reasonable results, especially with the addition of relative refractory period and spike-rate-adaptation mechanisms.

The *exponential Euler* integration scheme is applicable for the neuron models employed here as all differential equations have the form:

$$\frac{dy}{dt} = A(t) - B(t)y.$$

The solution at a time $t + dt$ is approximated in terms of the solution at time t by:

$$y(t + dt) = y(t)e^{-B(t)dt} + \frac{A(t)}{B(t)}(1 - e^{-B(t)dt}).$$

This method is stable, in contrast to the forward Euler method. It is the recommended integration scheme for the type of neuron simulations undertaken here [2, 10].

Shown in fig. 2.4 is a comparison of the two-neuron experiment results for NEURON ($dt = 0.01$ms), HANNEE forward Euler ($dt = 0.1$ms), HANNEE exponential Euler ($dt = 0.1$ms) and HANNEE exponential Euler ($dt = 0.25$ms). The forward Euler method exhibited divergence already for $dt > 0.125$ms, where as the exponential Euler method was stable even for $dt = 0.25$ms. The solution of the exponential Euler method with a step size of $dt = 0.1$ms shows a deviation of less than 3% from the NEURON solution with 1/10th the step size. This exponential Euler method with a step size of $dt = 0.1$ms is the configuration used for the simulations to follow.
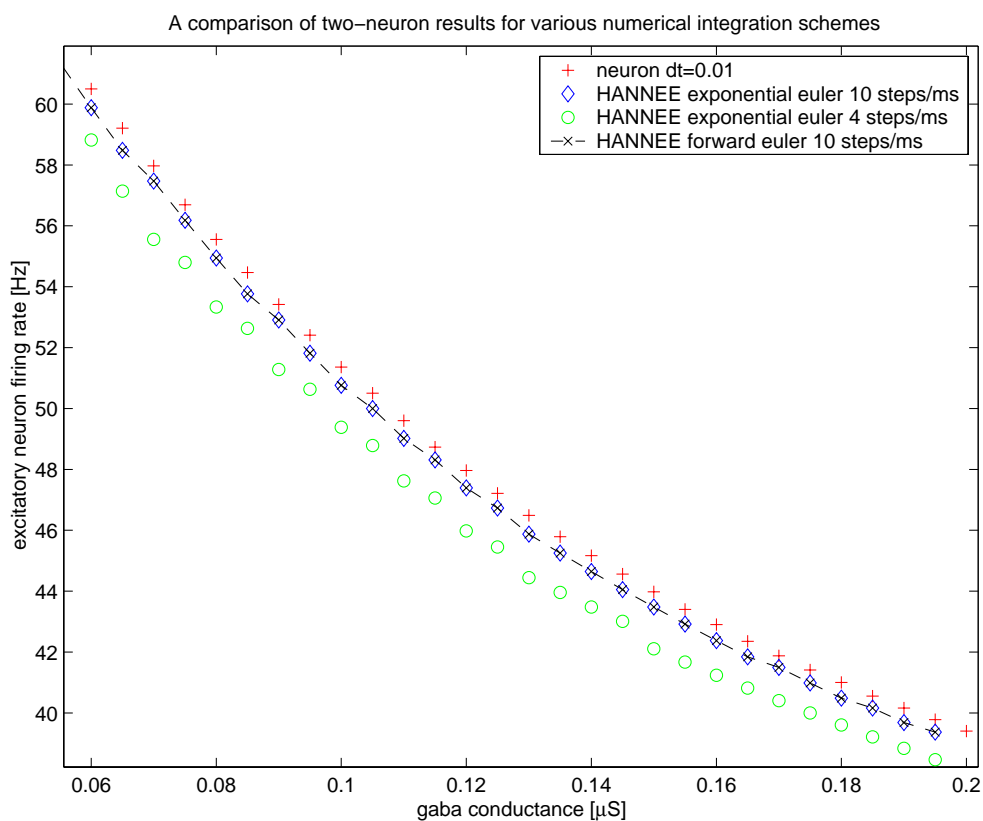
Figure 2.4: A comparison of the integration schemes implemented in HSimSpikeConData to the NEURON solution.

Chapter 3

Simulating Networks

The cortex of the mouse consists of approximately $2e7$ neurons, each with about 8000 synapses, spread over the outer brain surface of $\sim 90\text{mm}^2$ to a depth of $\sim 2\text{mm}$. The total number of input fibers is $< 1e6$. The axons extend $\sim 1\text{mm}$ from pyramidal cells and $\sim 0.2\text{mm}$ from inhibitory cells. At a density of $9e4$ cells/mm^3, pyramidal axons have access to $\sim 4e5$ other neurons in their neighborhood [15].

In simulation, under current computational limitations, we cannot expect to match the scale and complexity of a living mouse brain, let alone the human brain. Currently, ~ 1000 neurons of the highly simplified integrate-and-fire model can be simulated reasonably on a standard PC. Using Linux clusters currently available, this number could be increased by a factor of ~ 100. In this section. a network simulation system will be proposed that, while working under these computational limitations, still provides insight into emergence of global properties from local dynamical rules in a patch of a cortex-like neural network in an active awake state.

3.1   The High-Conductance State

Cortical neurons under awake conditions *in-vivo* are found to be characterized by low input resistance, depolarization, continuous membrane potential fluctuations and spontaneous firing, all features due mostly to opposing excitatory and inhibitory spontaneous synaptic activity [6]. This mode of operation is known as the *high-conductance state* of cortical neurons.

There are many approaches to induce a high-conductance state in simulation. Synaptic bombardment with Poisson process events, as done in the first section, was the method chosen here. Synaptic activity is generated by 1000 excitatory and 250 inhibitory Poisson processes with Poisson release rates of e and i respectively. For rates, (e,i), above a few Hz, the synaptically activated contribution to the membrane conductance becomes appreciable and the transition to the high-conductance state occurs.

The firing rate of the neuron in the high-conductance state is not so much determined by the magnitude of the conductance as by the balance between the excitatory and inhibitory background. This can be seen by introducing the total conductance, g_t, and the effective voltage, v_{eff}[1],

$$g_t = g_l + g_e(t) + g_i(t)$$

$$v_{eff} = \frac{g_l E_l + g_e(t) E_e + g_i(t) E_i}{g_t},$$

Where $g_{e,i}(t)$ is the sum of all excitatory,inhibitory synaptic conductances with reversal potential $E_{e,i}$

---

[1]This development follows that in [7].

(weights are uniformly unity). Eq. 1.1 then becomes:

$$c_m \frac{dv(t)}{dt} = g_t(v_{eff} - v(t)).$$ (3.1)

What is immediately clear by this formalism is that for synaptic conductances appreciable compared to the leak conductance, g_l, the membrane potential follows $v_{eff} \approx g_e(t)E_e + g_i(t)E_i$ with time constant $g_t \approx g_e(t) + g_i(t)$. Under synaptic bombardment v_{eff} performs roughly a random walk about it's mean, $\langle v_{eff} \rangle = \langle g_e \rangle E_e + \langle g_i \rangle E_i$, where firing occurs when v crosses v_{th} ($\langle \rangle$ denotes the time average). The balance of $\langle g_e \rangle$ and $\langle g_i \rangle$ then determines how close to the threshold v_{eff} performs its walk. How often v_{eff} crosses the threshold is determined by this closeness and the spread of v_{eff} about its mean. Since g_t determines how quickly v follows the walk of v_{th}, the firing rate of the neuron is determined by an interplay of the spread of v_{eff}, the balance of $\langle g_e \rangle$ and $\langle g_i \rangle$, and the total conductance g_t.

In practice, in a high-conductance state, the total conductance is high enough that v closely follows v_{eff}. Since quantal synaptic increases and synaptic time constants do not change for our purposes during the simulation, the spread of v_{eff} also remains constant. Thus the primary influence on the firing rate during the simulation is the balance of $\langle g_e \rangle$ and $\langle g_i \rangle$ which are monotonically increasing functions of the synaptic release rates, e and i respectively.

3.2   Neuron Coupling, Rate Maps and Model-Consistent Background Rates

The Poisson process synaptic bombardment during single neuron high-conductance experiments is an attempt to model the synaptic activity which would occur at the dendrites of the postsynaptic neuron given realistic *in-vivo* awake firing rates of its presynaptic neurons. In real cortical networks within a given layer the connections between neurons are roughly isotropic and densely interconnected [15]. Thus the the neurons that make up the "background" are also caused to fire by the "background". The two classes of neurons, pyramidal and inhibitory, have distinct firing rates which depend on the background excitatory and inhibitory firing rates themselves, as discussed in the previous section. These firing rates will in turn determine the firing rates of other neurons in the network. If realistic firing rates are to be preserved in this feedback mechanism, there is an issue of consistency to be resolved.

More specifically, the goal is to find exactly those background rates, e and i, which are reproduced in the average firing rates of the pyramidal and inhibitory neurons respectively, under synaptic bombardment experiments. These will be referred to from now on as the *model-consistent background rates* (MCB rates) as they are those rates for which the mean rate of the models are consistent with the mean background rates.

The first step made towards finding the model-consistent background rates is to map the mean firing rates of the pyramidal and inhibitory neuron models as a function of the background rates, e and i. Using NEURON, for background rates $e = 2 - 40$Hz, $i = 4 - 60$Hz and step-size 0.5Hz, each neuron model was bombarded for ten seconds of simulation time and the reciprocal mean ISI determined. The resulting rate maps are shown in fig. 3.1.

Then by employing custom MATLAB scripts, the MCB rates can be found, if they exist, using the reasoning as follows. Consider the functions

$$f(e, i) = f_{PY}(e, i) - e,$$

$$g(e, i) = f_{IN}(e, i) - i,$$

where e and i denote the background firing rates and $f_{PY}(e, i)$ and $f_{IN}(e, i)$ denote the rate maps of the pyramidal and inhibitory neuron, respectively, as estimated in the experiments previously. Let
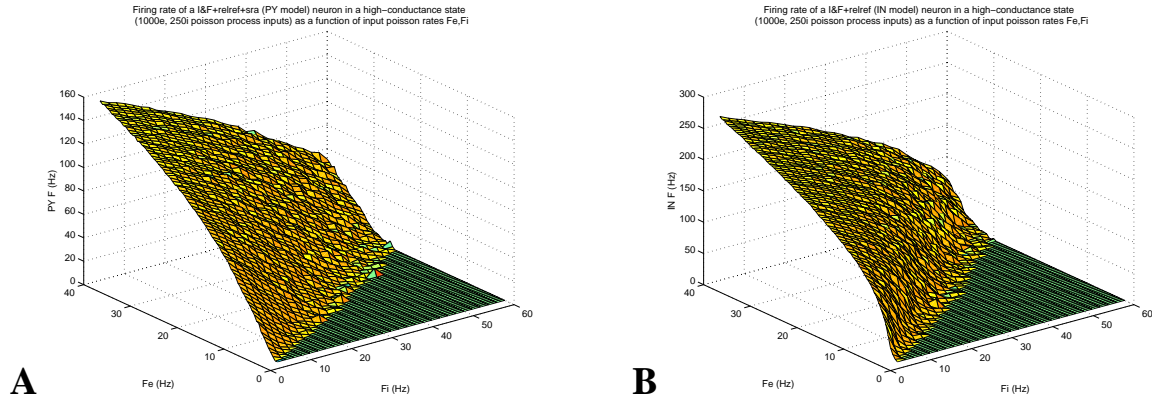
Figure 3.1: **A**: Reciprocal mean ISI as a function of synaptic bombardment background rates for the pyramidal neuron model. **B**: As in A, but for the inhibitory neuron model

$i^*(e)$ be the zero of $f(e, i)$ for a given e. Let e^{**} be the zero of $g'(e) = g(e, i = i^*(e))$. If e^{**} exists then it and $i^*(e^{**})$ are the MCB rates.

For the rate maps as show in fig. 3.1, $g'(e)$ and $i^*(e)$ were plotted against e, shown in fig. 3.2. Initially, a numerical search was done for the zero of $g'(e)$ yielding ($e = 8.9409$Hz, $i = 15.4918$Hz) for the choice of MCB rates.

Later, through plotting $g'(e)$, it became clear the numerical solution is not unique, as the random like variations of $g'(e)$ cause it to cross the e-axis several times. If one assumes that the variation in $g'(e)$ is statistical variation, a realistic assumption considering that the rate maps were generated using finite rate measurement times, then $g'(e)$ has an apparent linear form. A linear fit to $g'(e)$ is included in fig. 3.2. By this method the MCB rates were found to be ($e = 6 \pm 1$Hz, $i = 10.1 \pm 1.5$Hz). The MCB rates determined by both methods were considered in the simulations to follow.

As the MCB rates are those background rates which will be used to produce *in-vivo*-like high-conductance states in the neuron model, it is interesting and demonstrative to briefly investigate the effects of such background rates on the properties of the neuron model and verify that those properties observed in experiment actually do manifest. Shown in fig. 3.3 are the conductances and membrane potentials for the MCB pairs found using both methods. Experimental studies *in-vivo* have shown $\langle g_i \rangle / \langle g_e \rangle \approx 2$ to 6, with which the quantities observed here are in agreement, but on the lower end. Moreover, the close following of v_{eff} by v might not be as close as promised. Indeed, 1000 excitatory and 250 inhibitory synaptic inputs is a little on the low side when compared to biological quantities. Agreement might be improved if the number of inputs were doubled or tripled. For current purposes, however, the agreement will be considered sufficient.

3.3 Network Architecture

The approach taken to simulate an *in-vivo*-like cortical network was to employ a population of neurons, each of which is in a high-conductance state induced by Poisson process generated synaptic activity at the MCB rates (see previous section), and then to replace a percentage of the excitatory and inhibitory synaptic input of each neuron by activity originating from other pyramidal and inhibitory neurons in the network, respectively. Indeed, the injection of noise to activate the network serves as a biologically plausible boundary condition, as it roughly mimics the surrounding unmodeled neurons, and inputs from other layers of the cortex and other areas of the brain. Similar techniques have been used by D. McLaughlin in modeling the macaque primary visual cortex (V1) [16].
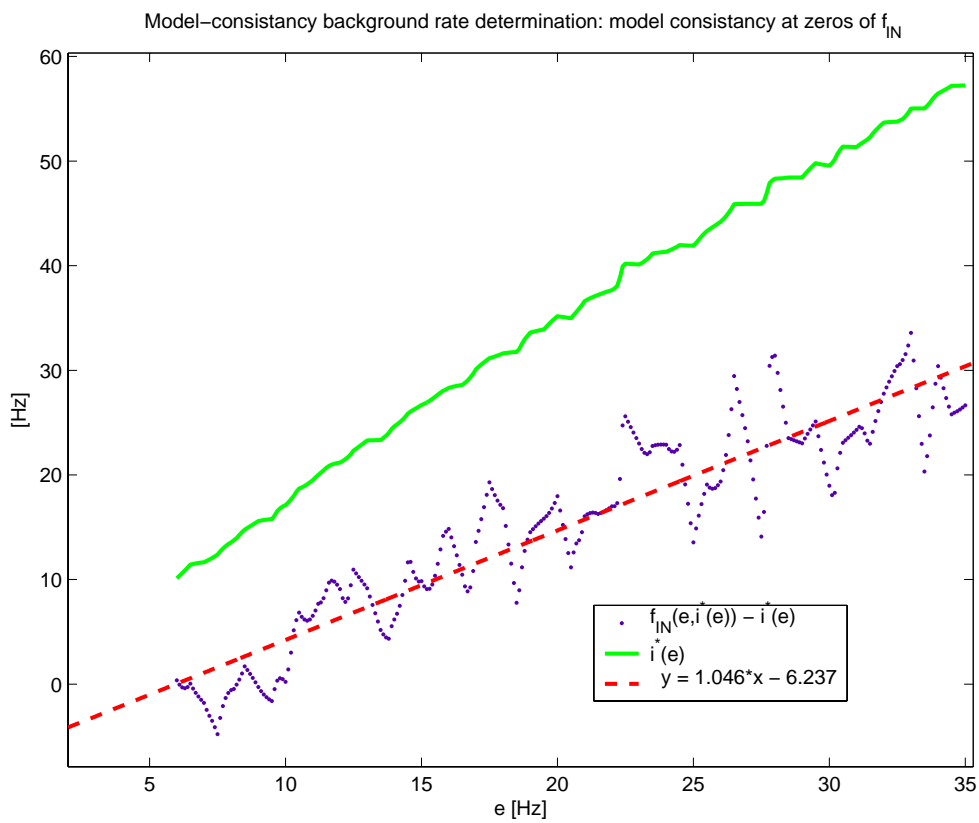
Figure 3.2: Determining the model-consistent background rates by zeros of $\not g(e)$: by numerical zero search ($e = 8.9409\text{Hz}$, $i = 15.4918\text{Hz}$), by linear fit ($e = 6 \pm 1\text{Hz}$, $i = 10.1 \pm 1.5\text{Hz}$).
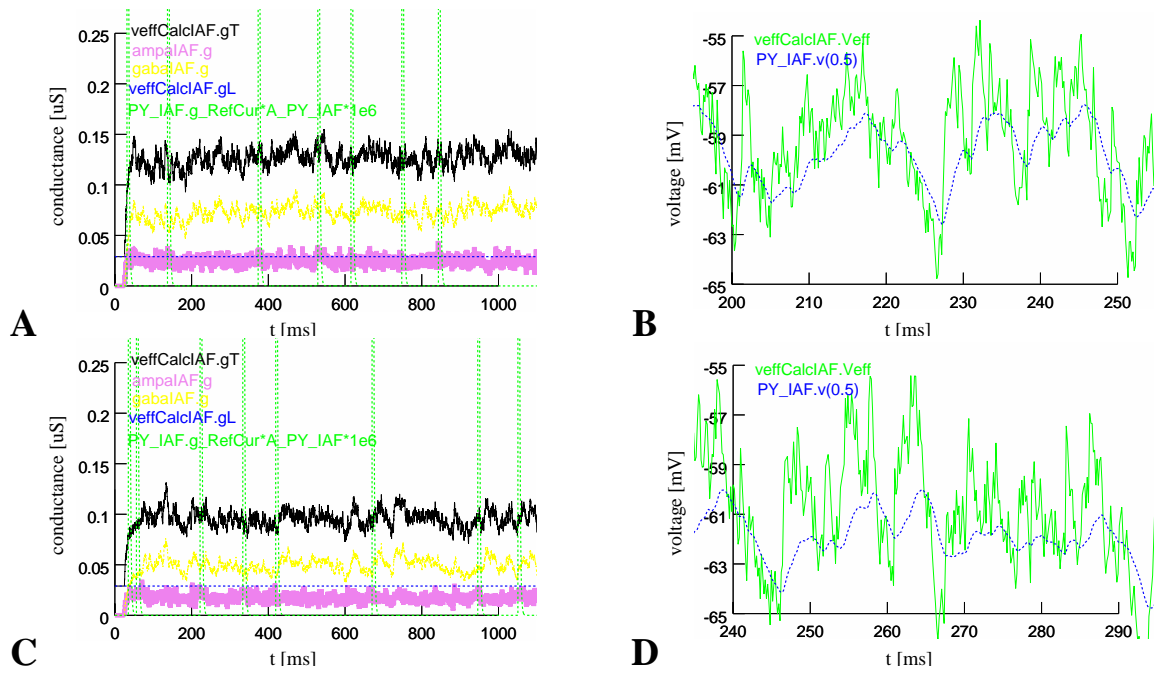
Figure 3.3: A high-conductance state induced by Poisson process synaptic bombardment (1000 excitatory, 250 inhibitory). **A**: numerical solution MCB rates ($e = 8.9409$Hz, $i = 15.4934$Hz), conductances. $\langle g_e \rangle \approx 0.9 \cdot g_l$, $\langle g_i \rangle \approx 2.7 \cdot g_l$, $\langle g_t \rangle \approx 4.5 \cdot g_l$. **B**: As in A, but for membrane potential and v_{eff}. **C**: linear fit MCB rates ($e = 6$Hz, $i = 10$Hz), conductances. $\langle g_e \rangle \approx 0.75 \cdot g_l$, $\langle g_i \rangle \approx 1.7 \cdot g_l$, $\langle g_t \rangle \approx 3.0 \cdot g_l$. **D**: As in C, but for membrane potential and v_{eff} .

In detail, a 9x9x9 grid of I&F neurons as described in chapter 1 was simulated. For any given neuron, it was presynaptic to n_{con} other neurons in the network, where n_{con} is drawn from a Poisson distribution with mean $r_{con} \cdot 9^3$ and r_{con} denotes to what fraction the network is fully connected. The postsynaptic neurons are drawn at random uniformly over the whole grid. Action potential transmission delays in the network are set as the Euclidean distance between neurons times the delay factor, f_{delay}. Whether a given neuron is inhibitory or pyramidal is determined by the inhibitory probability, p_{inhib}.

The network has two phases of operation: an *initiation phase* and a *run phase*.

1. Initiation phase: during this phase synapses between neurons in the network are disabled and each neuron is synaptically bombarded by 1000 excitatory and 250 inhibitory neurons as described in section 3.1. For $t = 0 - 100$ms the high-conductance state is allowed to establish. For $t = 100 - 600$ms the synaptic activity generated by the presynaptic inhibitory and pyramidal neurons respectively of each neuron is measured. The background rates, i and e are then decreased by exactly these measured inhibitory and pyramidal activities respectively.

2. Run phase: the network synapses are enabled and the simulation is allowed to run with the decreased background rates.

The simulation was implemented under the HANNEE framework as mentioned in chapter 2. All variables for each time step are stored in a time memory window, which is periodically written to disk to allow simulation lengths spanning multiple windows. Using this method, simulation duration is limited only by disk space. The output file format is the .mat MATLAB data file, allowing flexible data analysis under the MATLAB environment.

3.4   Network Simulation Results

For the control network simulation, the network model parameters were $r_{con} = 0.2$, $f_{delay} = 0.5$ms, $p_{inhib} = 0.2$, inspired from biologically realistic neuron and synapse density data. The neuron model parameters as in appendix A and the numerical solution MCB rates were used. The exponential Euler integration scheme was used with $dt = 0.1$ms. The simulation was run for 5 seconds simulation time, taking about 1 minute real-time for each 300 milliseconds of simulation time. A spiking activity plot for the entire network as a function of time is shown in fig. 3.4.

Of immediate interest is the periodic coherent network bursting observed, $\tau = 170 \pm 20$ms. Fig. 3.5C shows the conductances of a single neuron during such a network burst for the control simulation. The precise mechanism behind burst onset is yet unclear, however the mechanism is clearly disabled for a time by the adaptation induced in the pyramidal neurons during the burst. To demonstrate this fact, three more simulations were run with configurations as for the control, but with spike-rate-adaptation time constants, $\tau_{sra} = 20$ms, 65ms, 155ms (the control simulation has $t_{sra} = 110$ms). The observed dependence of the bursting period on t_{sra} is shown in fig. 3.5F. A slope of approximately unity indicates the bursting period is indeed determined exactly by τ_{sra} where the non-zero y-intercept is the burst width. That the data point for $\tau_{sra} = 20$ms lies off the fit line with a large variance is to be expected as the adaptation induced delay following a burst is, in this case, shorter than the burst width. Thus, the mechanism by which the burst is terminated is qualitatively different for this experiment. As shown in fig. 3.5E, the adaptation conductance falls almost as rapidly as the inhibition conductance, and it falls to zero without the onset of a new burst, in contrast to the control. Indeed, further investigation of this short adaptation regime might provide insight into the mechanism of burst onset.

The effects of changes in the network model parameters r_{con}, f_{delay}, p_{inhib} as well as in the network inhibitory synaptic decay time $\tau_{s,i}$ on the bursting properties of the network were investigated. Shown in fig. 3.6 is a comparison of the network synaptic conductances of a single neuron to those of the
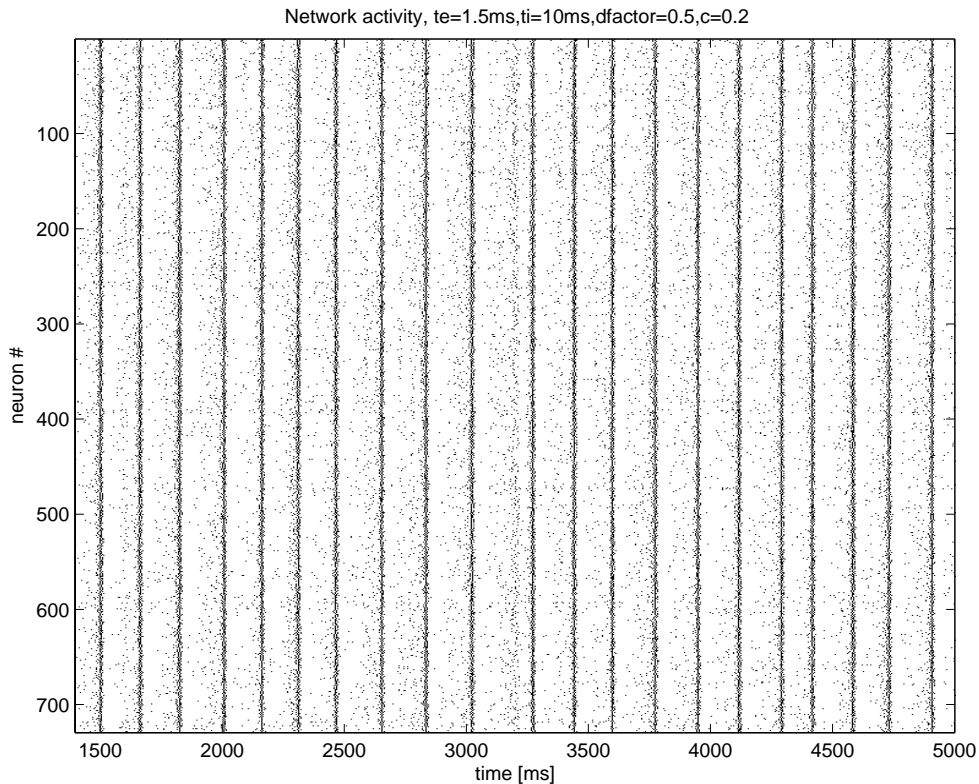
Figure 3.4: Spiking activity diagram for 5 seconds of simulation with $r_{con} = 0.2$, $f_{delay} = 0.5$, $p_{inhib} = 0.2$ and numerical MCB rates. A pixel indicates a spike occurred for that neuron at that time. The image is resolution decimated in time by summing the spike count of 50 time bins and placing it into 1. In this way the 50000 pixel wide image is reduced to 1000 pixels wide without loss of average spike activity due to spike loss from sub-sampling. Periodic coherent bursting of the network is observed with period $\tau = 170 \pm 20$ms.

control simulation under the said changes for the entire 5s simulation length. Shown in fig. 3.5A-D are the same comparisons at higher temporal resolution. The observed effects of the changes will now be discussed in turn.

For a reduction in the network inhibitory synaptic decay constant from $\tau_{s,i} = 10$ms to $\tau_{s,i} = 5$ms, the network bursting period is seen to increase, shown in fig. 3.6D and 3.5D. At first glance this is somewhat counter-intuitive result, however on closer examination, one sees that the inhibitory conductance peaks during burst events reach only two thirds those of the control simulation. As inhibition likely breaks the excitatory avalanche occurring at bursting, a reduction of that inhibition would allow a slightly longer avalanche with a greater accumulation of adaptation conductance. The increase in time required for the larger adaptation to decay to a level allowing again burst onset is then observed as an increase in burst period. This fact can be seen without a doubt on closer inspection of fig. 3.5D.

For an increase in r_{con} from 0.2 to 0.4, a $3 - 4$ fold increase in peak excitatory and inhibitory conductance during burst events is observed, as shown in fig. 3.6B and 3.5B. The added connectivity in the network means AP events from single neurons are sent to twice as many postsynaptic neurons in the network as for the control, and thus significantly more excitatory and inhibitory activity is generated. This does not, however, directly explain the drastic increase in number of firing events per neuron during a network burst event as the ratio of excitatory to inhibitory activity and thus ψ_h increases only slightly. What does change drastically during the burst event is the total conductance, g_t, of the individual neurons. Because of this, the time constant by which the membrane potential follows the effective voltage is significantly decreased and thus many more AP events can occur over a shorter period of time, when v_{eff} is above the firing threshold. This increase in the number of firing events per neuron during a burst results in a similar accumulation of adaptation conductance as was seen in the previous example, though to a much higher degree, as seen in fig. 3.5B. Thus a greater increase in the bursting period is observed.

For an increase in f_{delay} from 0.5ms to 1.0ms, it seems the avalanche onset mechanism is impeded, as shown in fig. 3.6A and 3.5A. Occasionally it seems to be so impeded that burst onset fails, thus explaining the breakdown in periodicity observed. Further investigation of the effects of delays in the network might provide insight into the mechanism of burst onset.

The ISI histogram for single neurons in the various network configurations, shown in fig. 3.7A, is of interest as it can be directly compared with ISI histogram measurements of awake animals *in-vivo*. Although the number of trials is small, clearly bursting is causing a buildup of shorter ISIs for the network experiments. This non-gamma-like behavior of the ISI histogram for individual neurons in the network is in contradiction with the observed ISI histograms of cortical pyramidal neurons in awake animals *in-vivo* [1, ch. 15]. Simulation of a larger network with realistic variation of neuron parameters might produce better agreement.

To investigate the possibility of heterogeneity in network activity directly preceding burst events, the spike-time relative to burst onset was histogrammed as a function of neuron, shown in fig. 3.7B,C. No significant inhomogeneities were observed, hinting that burst onset is a communal building of activity rather than an event traceable to a specific cause.

3.5   Variations

An alternative approach to the background-rate-reduction scheme used for the network init phase described in section 3.3 is a neuron-for-neuron replacement scheme:

1. Initiation phase: during this phase synapses between neurons in the network are disabled and each neuron is synaptically bombarded by 1000 excitatory and 250 inhibitory neurons as described in section 3.1. For $t = 0 - 100$ms the high-conductance state is allowed to establish. Then, the number of excitatory and inhibitory neurons used to generate the background is for
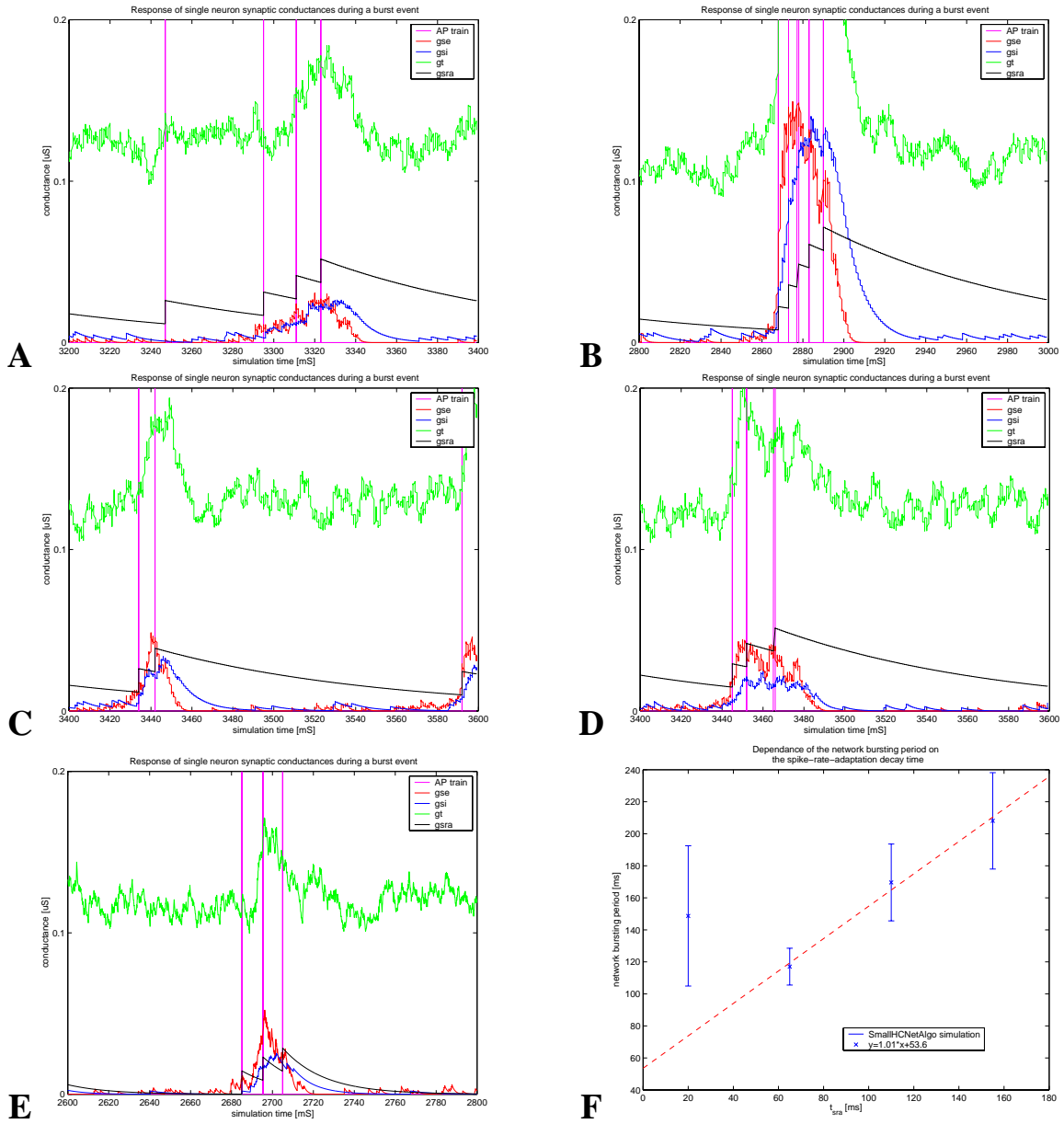
Figure 3.5: Conductances of a single neuron during a coherent network burst event. (red) gse - excitatory synaptic activity originating from network neurons, (blue) gsi - same as gse but inhibitory, (black) gsra - spike-rate-adaptation conductance, (green) gt - total conductance including background activity but neither gsra nor grelref, (magenta) AP train - vertical lines indicate those times an action potential was generated by the neuron. Deviation from control parameters as indicated. **A**: $f_{delay} = 1.0$ms. **B**: $r_{con} = 0.4$. **C**: control. **D**: network inhibitory synaptic decay time, $\tau_{s,i} = 5$ms. Background inhibitory synaptic decay time remained unchanged at 10ms. **E**: $\tau_{sra} = 20$ms. **F**: Dependence of coherent network bursting period on τ_{sra}.
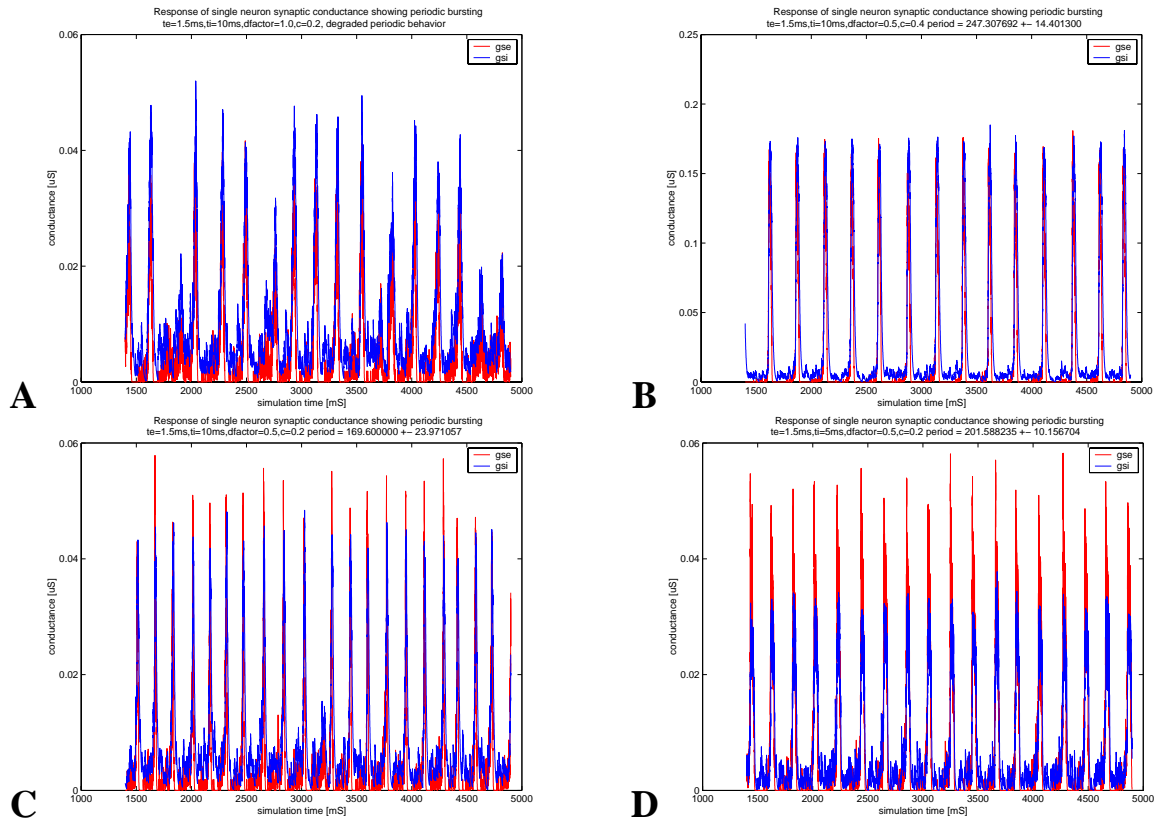
Figure 3.6: Synaptic conductances due to network neurons: (red) gse - excitatory, (blue) gsi - in-hibitory. Peaks in conductance occur at network burst events. Bursting periods are indicated in the plots. Changes from control simulation parameters are as indicated. **A**: $f_{delay} = 1.0$ms. **B**: $r_{con} = 0.4$. **C**: control. **D**: network inhibitory synaptic decay time, $\tau_{s,i} = 5$ms. Background in-hibitory synaptic decay time remained unchanged at 10ms.
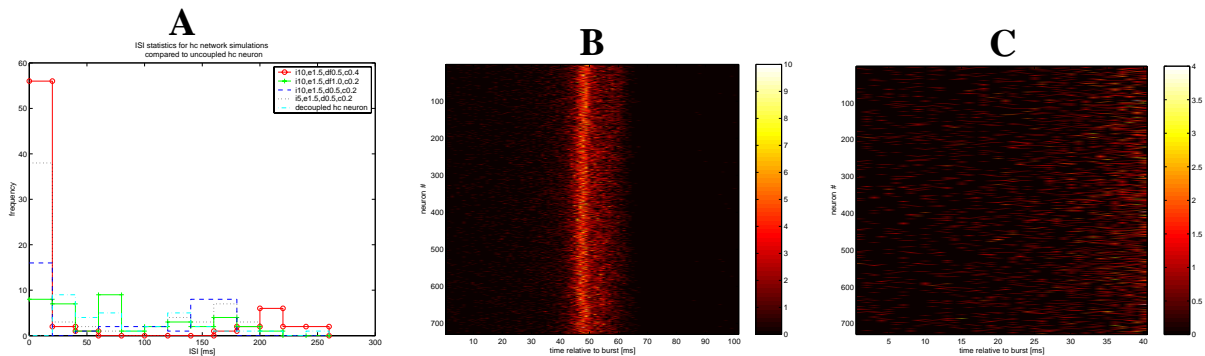

Figure 3.7: **A**: A comparison of ISI histograms for single neurons in various network configurations. **B**: A plot showing the distribution of spiking activity among neurons relative to burst time, summed over all bursts. Network and neuron parameters as control, linear fit MCB rates, neuron-for-neuron init scheme. **C**: Same as in B, rescaled to show the burst onset region.

each neuron reduced by exactly the number of network pyramidal and inhibitory neurons to which it is postsynaptic, respectively.

2. Run phase: the network synapses are enabled and the simulation is allowed to run.

One could argue that the neuron-for-neuron replacement scheme is superior. Assuming the background is firing at the MCB rates, Poisson process background neurons and network neurons are interchangeable. This is true to a high degree of accuracy as the MCB rates were calculated using rate map measurements with simulation times of 10000ms per data point. In contrast, the background-rate-reduction init scheme of section 3.3 measures for only 500ms to get an estimate of the neuron firing rates, where the background rates are then reduced by exactly those amounts which leave excitatory and inhibitory activity unchanged following network synapse activation. For firing rates of 10Hz, indeed these estimates will be inaccurate. For network and neuron configurations as the control, a simulation using the neuron-for-neuron replacement init scheme was run. The spiking activity plot is shown in fig. 3.8. Coherent network bursting is observed with period $\tau = 107 \pm 8$ms. There is a clear deviation from the bursting period of the same experiment using the background-rate-reduction init scheme. The cause of this inequivalency is likely the short measurement time in the background-rate-reduction scheme and the errors it induces. It could however be due to error in the numerical solution MCB rates. One could argue that the background-rate-reduction scheme is superior in that it would be more robust under such an error, as it does not replace neuron for neuron, but measures actual network activity and then reduces background by measured amounts. Also the neuron-for-neuron replacement scheme is a global operation, whereas the background-rate-reduction scheme is local. The background-rate-reduction scheme is therefore more likely to have a biological analog (synaptic plasticity?).

As of yet, all simulations have used the MCB rates determined by numerical solutions. As discussed in section 3.2, these MCB solutions are not unique and are susceptible to the statistical variation in the rate maps. The MCB rates as determined by a linear fit to $\dot{g}(e)$ likely remedies some of these issues. To investigate the effects of choice of MCB rates, the simulation was run using control network and neuron parameters, the linear fit MCB rates and the neuron-for-neuron init scheme. The spiking activity plot is shown in fig. 3.9. Coherent network bursting is observed with period $\tau = 180 \pm 20$ms, which is consistent with the bursting frequency observed for the control experiment using the background-rate-reduction scheme and the numerical MCB solution. The fact that background-rate-reduction scheme measures the necessary background frequencies changes at runtime means it is likely robust under small variation in the MCB rates. The neuron-for-neuron init scheme depends on accurate MCB rates for correct operation. That the simulations using neuron-for-neuron scheme with linear fit MCB rates and the background-rate-adjustment with numerical solution MCB rates agree for bursting period is indicative. Moreover, peak conductances during bursting and burst width and shape were found to be consistent. The preliminary conclusion is that the network state established using these two methods is consistent and that the MCB rates determined using the linear fit method are superior. As the properties of the neurons under synaptic bombardment at the linear fit MCB rates manifested only border-line high-conductance properties, further work should include simulations with double or triple the number of synapses to bring the neurons deeper into the high-conductance regime.
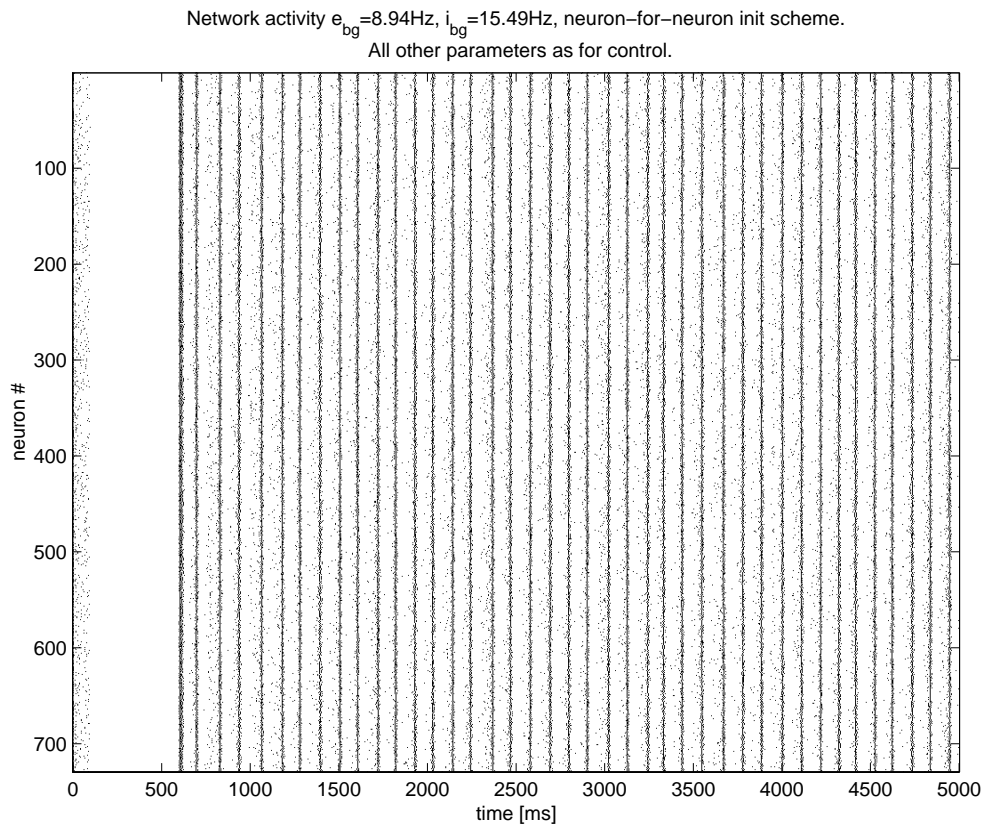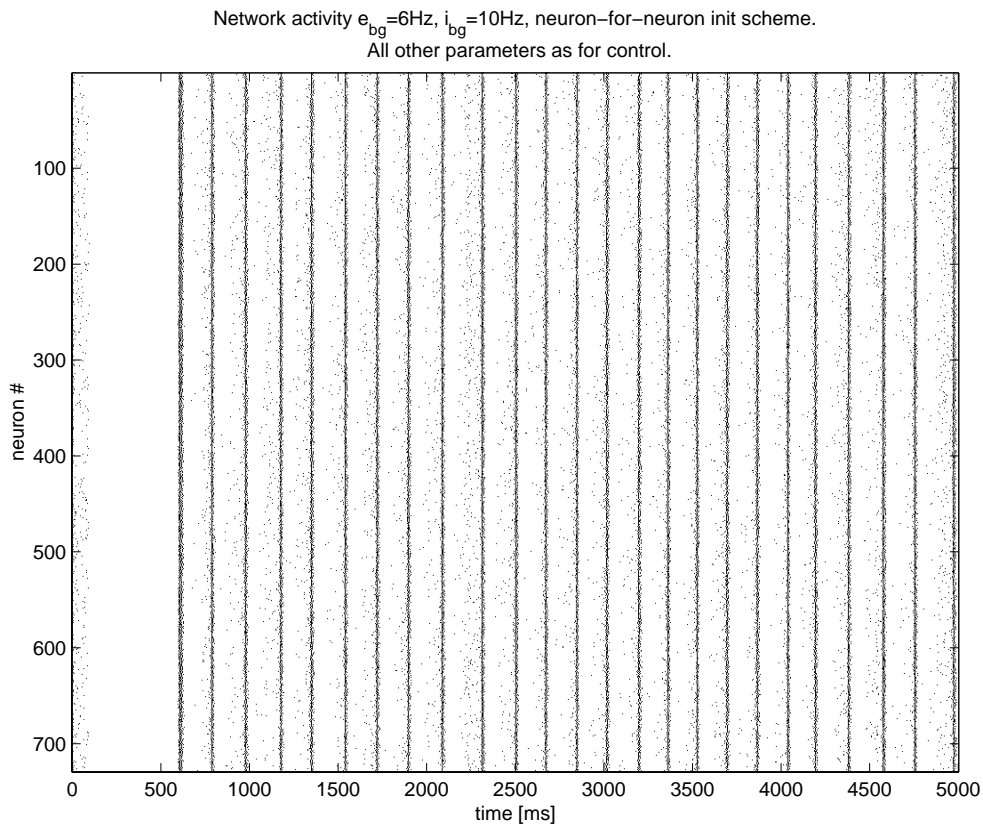
Figure 3.8: Spiking activity diagram for 5 seconds of simulation . A pixel indicates a spike occurred for that neuron at that time. The image is resolution decimated in time by summing the spike count of 50 time bins and placing it into 1. In this way the 50000 pixel wide image is reduced to 1000 pixels wide without loss of average spike activity due to spike loss from sub-sampling. Periodic coherent bursting of the network is observed with period $\tau = 107 \pm 8$ms.

Figure 3.9: Spiking activity diagram for 5 seconds of simulation . A pixel indicates a spike occurred for that neuron at that time. The image is resolution decimated in time by summing the spike count of 50 time bins and placing it into 1. In this way the 50000 pixel wide image is reduced to 1000 pixels wide without loss of average spike activity due to spike loss from sub-sampling. Periodic coherent bursting of the network is observed with period $\tau = 180 \pm 20$ms.

Chapter 4

Conclusion and Outlook

A cortical neural network simulation was designed and implemented which focused on replicating the high-conductance (HC) states of the individual neurons as observed during awake measurements *in-vivo*, while conforming to computational restrictions.

The integrate-and-fire model (I&F) for the neuron was used, with additional mechanisms to account for adaptation and non-absolute refractory periods. Neuron model parameters were determined by fitting it to a more detailed Hodgkin-Huxley based model. The parameters used during the network simulations are summarized in appendix A. The synapses were modeled using a conductance based approach. The high-conductance state was established for the neuron model by synaptic bombardment with 1000 excitatory and 250 inhibitory Poisson process synapses with quantal conductances of $q = 0.002\mu S$.

A 9^3 lattice of partially interconnected neurons in high-conductance states was simulated by injection of Poisson process events into the system. The idea of model-consistent-background (MCB) rates was introduced to solve the "a neuron is its own background" problem in networks with persistent activity. Two methods for bringing the network to an active state were proposed and tested. Periodic bursting on the order of $\sim 5 - 7$Hz was observed which was preserved over mild variation of all network parameters that leave the MCB rates unchanged.

The simulation software is an expansion of the HANNEE framework custom written in C++. Event based synapses mean signaling bandwidth requirements are low and a Linux cluster implementation is anticipated. The simulation was a factor 200 slower than real-time for the 9^3 lattice on a standard PC.

The time scale of bursting was demonstrated to be determined by the decay constant of adaptation, where the relation was linear with a slope consistent with unity. However, an explanation for the occurrence of bursts, i.e. the mechanism behind burst onset, is decidedly absent. Moreover, some have asserted that the bursting state observed is in fact undesirable and that other modes of operation should be sought in which it is absent [17, 18]. Firstly, this is likely not possible for this size of network without additional mechanisms if an active state is to be maintained. Secondly, during periodic bursting, where adaptation plays a role in burst termination, the strong adaptive currents incurred during the burst play a dissipative role in the network. This points towards an analogy for energy in the network, and suggests bursting could be eliminated by an outflow of energy, an additional dissipative mechanism, or an equilibrating mechanism. The first possibility is undesirable as it would leave the network inactive. The last possibility is likely the most plausible if indeed bursting is objectionable.

The possibilities however for manifesting computational mechanisms through bursting should not go unmentioned. Firstly, due to sparse interconnections between differing layers and differing parts of the brain, signaling through these channels is likely only possible through strong, coherent activity from the emitting side. Secondly, considering heterogenous connectivity in the cortex determined by complex but semi-local rules, bursting could represent a sort of communal emergent decision of a large population of diverse entities working in a massively parallel fashion. Here the diversity

and structure inherent in the interconnections would be of vital importance. Certainly, investigating the global effects of local connection rules would be an interesting application of a neural network simulation, however the outlook is dim if simulation of tiny volumes of cortex remains state-of-the-art.

Indeed, the current network size limitations of the simulation may play an important role in the creation of artifact bursting. Just as a water droplet skims the same surface where quantities of water would boil, a change of scale and the addition of degrees of freedom can drastically alter the dynamics of a system. Where the emergent excited modes of liquid water at large enough scales are turbulence and convection, autonomous intelligence is the emergent excited mode of the structured hyper-liquid[1] based computer that is the cortex. Certainly mere activity propagation experiments at the scale of the simulation here are unthinkable. Attempts to solve the "to burst or not to burst" question will be postponed until this condition is improved. A Linux cluster implementation should better the situation but would be too slow for the necessary parameter searches allowing investigation of the yet unfathomable dynamics. Ultimately, a scalable interactive hardware approach should be the target modeling platform, fast enough to grind out the incalculable design parameters of such large networks using genetic algorithms and their variants.

The role of simulation in the mean time could be to expand our imagination to the ever more dazzling array of modes of dynamical operational which the cortical hyper-liquid represents. Key will be the achievement of a large enough scale, simulation of diversity in elemental substrate and in dynamical mechanisms such as synaptic plasticity and neuromodulation, visualization techniques and data abstraction, and an ever expanding knowledge base through examination of the biological artifacts.

---

[1]This compelling analogy was inspired by the theoretical elaborations of the *liquid computing* paradigm in [5]. The word *hyper* was haphazardly prepended, in the context of this analogy, to distinguish the vast and elusive dynamical possibilities of the cortex from the relative simplicity of everyday water.

Appendix A

Complete I&F Model and Parameters

The exact membrane potential as it is simulated in HANNEE, unless otherwise stated, is governed by the equation:

$$c_m \frac{dv(t)}{dt} = g_l(E_l - v(t)) + g_{sra}(t)(E_{sra} - v(t)) + g_{relref}(t)(E_{relref} - v(t))$$
$$+ g_e(t)(E_e - v(t)) + g_i(t)(E_i - v(t)) + \sum_j \frac{w^j g_s^j(t)}{A}(E_s^j - v(t)).$$

If v exceeds v_{th}:

- v is reset to v_{reset}.

- Synaptic release events are triggered at the neuron's synapses, k, following individual synaptic delays: g_s^k becomes $g_s^k + q_s^k$. Note: k was used here instead of j to distinguish the input synapses in the membrane equation above from these k synapses to which this neuron is presynaptic.

- g_{sra} becomes $g_{sra} + q_{sra}$.

- g_{relref} becomes $g_{relref} + q_{relref}$.

All currents, $g_X(t)$, where $X \epsilon \{relref, sra, e, i, s^j\}$ are governed by an equation of the form:

$$\frac{dg_X(t)}{dt} = \frac{-1}{\tau_X} g_X(t).$$

Release events at the Poisson process background synapse conductances, $g_e(t), g_i(t)$ are generated by 1000 (excitatory), 250 (inhibitory) Poisson processes. Events have exponentially distributed ISI histograms with mean determined by background rates e, i. At the time of an event $g_{e,i}$ becomes $g_{e,i} + q_{e,i}$.

Choice of parameters unless otherwise stated:

- $v_{th} = -57$mv - threshold voltage

- $v_{reset} = -70$mv - reset voltage

- $c_m = 10$nF/mm^2 - specific membrane capacitance

- $g_l = 1.0\mu$S/mm^2 (pyramidal), 1.5μS/mm^2 (inhibitory) - specific membrane leak conductance

- $E_l = -70$mv - membrane reversal potential

- $E_s^j = 0$mv (pyramidal), -75mv (inhibitory) - reversal potential of synapse j

- $w^j = 1.0$ - network synaptic weight

- $q_s^j = 0.002\mu$S - network synaptic quantal conductance increase

- $\tau_s^j = 1.5$s (pyramidal), 10.0s (inhibitory) - network synaptic decay time

- $t_{delay}^j = $ distance dependant, see section 3.3 - presynaptic-neuron-to-synapse AP propagation delay

- $A = 0.028953$mm^2 (pyramidal), 0.014103mm^2 (inhibitory) - membrane surface area

- $q_{relref} = 3.214\mu$S - relref quantal conductance increase

- $\tau_{relref} = 1.97$ms - relref conductance decay time

- $E_{relref} = -70$mv - relref reversal potential

- $q_{sra} = 0.01448\mu$S - sra quantal conductance increase

- $\tau_{sra} = 110$ms - sra conductance decay time

- $E_{sra} = -70$mv - sra reversal potential

- $q_{e,i} = 0.002\mu$S - Poisson process synaptic quantal conductance increase

- $\tau_{e,i} = 1.5$s (excitatory), 10.0s (inhibitory) - Poisson process synaptic decay time

- $E_{e,i} = 0$mv (excitatory), -75mv (inhibitory) - reversal potential of background synapses

Bibliography

[1] Christof Koch. *Biophysics of Computation: Information Processing in Single Neurons.* Oxford University Press, 1999.

[2] Peter Dayan and L.F. Abbott. *Theoretical Neuroscience: Computational and Mathematical Modeling of Neural Systems.* The MIT Press, Cambridge, Massachusetts, 2001.

[3] Wulfram Gerstner and Werner Kistler. *Spiking Neuron Models: Single Neurons, Populations, Plasticity.* Cambridge University Press, 2002.

[4] M.L. Hines and N.T. Carnevale. The neuron simulation environment. *Neural Computation*, 9:1179–1209, 1997.

[5] W. Maass, T. Natschläger, and H. Markram. Real-time computing without stable states: A new framework for neural computation based on perturbations. *Neural Computation*, 14(11):2531–2560, 2002.

[6] Alain Destexhe, Michael Rudolph, and Denis Paré. The high-conductance state of neocortical neurons in vivo. *Nature Reviews Neuroscience*, 4:739–751, 2003.

[7] M. Shelley, D. McLaughlin, R. Shapley, and D.J. Wielaard. States of high conductance in a large-scale model of the visual cortex. *Journal of Computational Neuroscience*, 13:93–109, 2002.

[8] M. Rudolph and A. Destexhe. The discharge variability of neocortical neurons during high-conductance states. *Neuroscience*, 2003.

[9] André Longtin, Adi Bulsara, and Frank Moss. Time-interval sequences in bistable systems and the noise-induced transmission of information by sensory neurons. *Phys. Rev. Let.*, 67(5):656–659, 1991.

[10] Alexander D. Protopapas, Michael Vanier, and James M. Bower. Simulating large networks of neurons. In Christof Koch and Idan Segev, editors, *Methods in Neuronal Modeling: From Ions to Networks*, chapter 12. The MIT Press, Cambridge, Massachusetts, second edition, 2001.

[11] Sen Song, Kenneth D. Miller, and L. F. Abbott. Competitive hebbian learning though spike-timing-dependent synaptic plasticity. *nature neuroscience*, 3(9):919–926, 2000.

[12] David. A. McCormick, Zhong Wang, and John Huguenard. Neurotransmitter control of neocortical neuronal activity and excitability. *Cerebral Cortex*, 3(5):387–398, 1993.

[13] `http://www.cnl.salk.edu/~alain/`.

[14] Walter M. Yamada, Christof Koch, and Paul R. Adams. Multiple channels and calcium dynamics. In Christof Koch and Idan Segev, editors, *Methods in Neuronal Modeling: From Ions to Networks*, chapter 4. The MIT Press, Cambridge, Massachusetts, second edition, 2001.

[15] Valentin Braitenberg and Almut Schüz. Cortex: hohe ordnung oder größtmögliches durcheinander. *Spektrum der Wissenschaft*, 1989.

[16] David McLaughlin, Robert Shapely, Michael Shelley, and D.J. Wielaard. A neuronal network model of macaque primary visual cortex (v1): Orientation selectivity and dynamics in the input layer 4cα. *PNAS*, 97(14):8087–8092, 2000.

[17] W. Gerstner. Personal communication, September 2003.

[18] A. Destexhe. Personal communication, September 2003.

Acknowledgments

Statement of Originality (Erklärung)

I certify that this thesis, and the research to which it refers, are the product of my own work, and that any ideas or quotations from the work of other people, published or otherwise, are fully acknowledged in accordance with the standard referencing practices of the discipline. I certify that this thesis has not been submitted for a higher degree to any other University or Institution.

(Deutsch) Ich versichere, dass ich diese Arbeit selbständig verfasst und keine anderen als die angegebenen Quellen und Hilfsmittel benutzt habe.

Heidelberg, 17.09.2003

....
(signature)